Supporting Information for

Multifunctional phase change composites for green electromagnetic interference shielding and thermal response prepared under the guidance of impedance matching strategy

Jie He[a, b], Jiaozu Wu[b], Chul B. Park[b, c], Pengjian Gong[b*], Chaobo Liang[d *], Guangxian Li[b]

[a] School of Aeronautics and Astronautics, Sichuan University, Chengdu 610065, China

[b] State Key Laboratory of Polymer Materials Engineering, College of Polymer Science and Engineering, Sichuan University, Chengdu 610065, China

[c] Microcellular Plastics Manufacturing Laboratory, Department of Mechanical and Industrial Engineering, University of Toronto, Toronto M5S 3G8, Canada

[d] Key Laboratory of Functional Nanocomposites of Shanxi Province, College of Materials Science and Engineering, North University of China, Taiyuan 030051, China

[*] Corresponding authors.

E-mail addresses: pgong@scu.edu.cn (P. Gong), lcb@nuc.edu.cn (C. Liang).

Section S1: Materials, Methods, and Characterization

Section S2: Supplementary Figure. S1-S22, and Table S1-S5

Section S1: Materials, Methods, and Characterization

Materials: Pyromellitic dianhydride (PMDA), 4,4′-oxydianiline (ODA), Dimethylacetamide (DMAc), Triethylamine (TEA), Polyvinylpyrrolidone (PVP), silver nitrate (AgNO₃), iron trichloride hexahydrate (FeCl₃·6H₂O), polyethylene glycol (PEG), Benzene-1,3,5-tricarboxylic acid (H₃BTC), N,N-Dimethylformamide (DMF), Nickel(II) nitrate hexahydrate (Ni(NO₃)₂·6H₂O) were all supplied by Sinopharm Chemical Reagent Co., Ltd. Methanol and ethanol were purchased from Shanghai Macklin Biochemical Technology Co., Ltd. GO dispersion was obtained from Changzhou Sixth Element Material Technology Co., Ltd. All chemicals were analytical grade and used without further purification.

Methods:

Synthesis of polyamide acid (PAA)

First, 4.31 g of 4,4'-oxydianiline was added to a beaker containing 50 ml of dimethylacetamide and dissolved, after dissolving 4.7 g of pyromellitic dianhydride in the above mixture. The reaction temperature was maintained at 20°C with mechanical stirring until complete dissolution. Then, equal molar ratio of triethylamine was added to the above mixture, and the PAA solution was obtained by vigorous mixing. Finally, PAA powder (precursor of PI) was obtained by lyophilization at -72°C for 48 h.

Synthesis of Ni-MOF

The Ni-MOF was prepared according to the previous solvent synthesis method. First, 0.43 g of Ni(NO₃)₂·6H₂O was dissolved in 30 ml of mixture of DMF, water, and ethanol under magnetic stirring. Another solution was prepared by dissolving 0.15 g of H₃BTC and 1.0 g of PVP in further 30 ml of mixed solution. Eventually, mixed solution reacted at 150°C for 10 h. The precursor was obtained by centrifugation several times.

Synthesis of AgNW

Our previous work detailed a polyol synthesis method for AgNW. 0.544 g silver nitrate was dissolved in 40 ml ethylene glycol. 0.55 mg $FeCl_3 \cdot 6H_2O$ and 0.57 g PVP were mixed with another 40 ml ethylene glycol. The above solution is mixed drop by drop and then transferred to an autoclave, where it reacted at 160°C for 150 minutes. Finally, AgNW obtained by centrifugation several times.

Characterization: Scanning electron microscopy (SEM) images of aerogels were analyzed by Hitachi SU8010 field emission scanning electron microscope at an accelerating voltage of 5 kV (Hitachi Corp., Japan). Energy-dispersive X-ray spectroscopy was employed to analyze the distribution of elements (Hitachi Corp., Japan). And the infrared images of the composites were obtained by Fluke Ti400 infrared thermal imager (Fluke Corp., America). Thermal conductivity and magnetic saturation strength of the aerogels were obtained by Hot Disk TPS-2500s (Hot Disk AB Corp., Sweden) and PPMS 9T (Quantum Design Corp., America).The electrical conductivity of carbon aerogels was evaluated by using Qianfeng SB120 four-point probes meter at room temperature (Qianfeng Corp., China). The densities of the carbon aerogels were determined by measuring the volume and weight of the samples. Fourier transforms infrared (FTIR) spectra was measured on a Nicolet 6700 spectrometer in the 4000-500 cm^{-1} (Thermo Fisher Scientific Corp., USA). Crystallography was obtained by DX-2700B X-ray diffraction (XRD, Haoyuan Corp., China). All of the carbon aerogels were backfilled with epoxy and then carved into rings with an outer diameter of 7 mm and an inner diameter of 3.04 mm by an engraver. The permittivity and

permeability are calculated using the S parameters obtained by a vector network analyzer (VNA, Agilent N5232) within the rang. The measurements of EMI shielding performance were performed on N5230 vector network analyzer (Agilent Corp., America). EMI SE_T, EMI SE_A, EMI SE_R, T, A and R were calculated from the S parameters according to the following equations:

$$R = |S_{11}|^2, T = |S_{21}|^2$$

$$A = 1 - R - T$$

$$SE_R = -10log_{10}(1 - R)$$

$$SE_A = -10log_{10}(\frac{T}{1 - R})$$

$$SE_T = SE_R + SE_A + SE_M$$

The multiple-reflection SE (SE_M) can be ignored when the SE_T is beyond 15 dB.

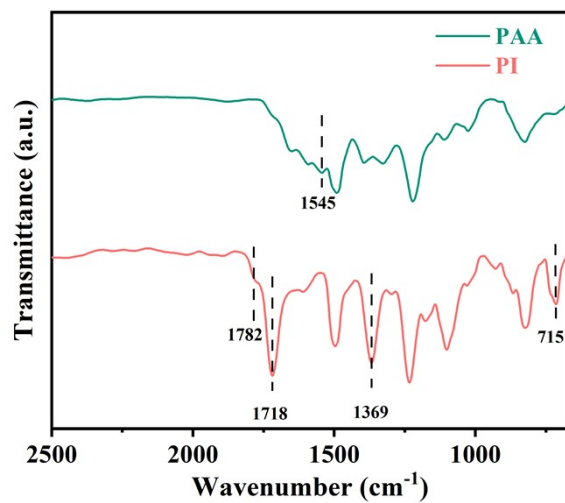**Section S2: Supplementary Fig. S1-S22, and Table S1-S5**

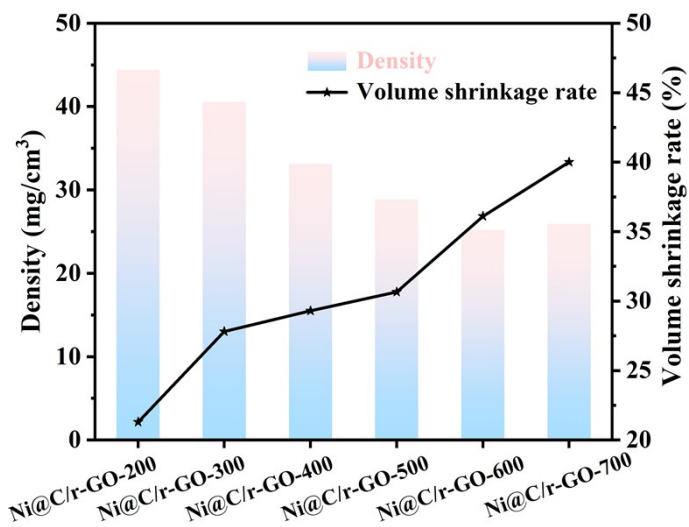**Figure S1** FTIR spectra of the PAA and PI.

Figure S2 The Volume shrinkage ratio and Density of Ni@C/r-GO-X.

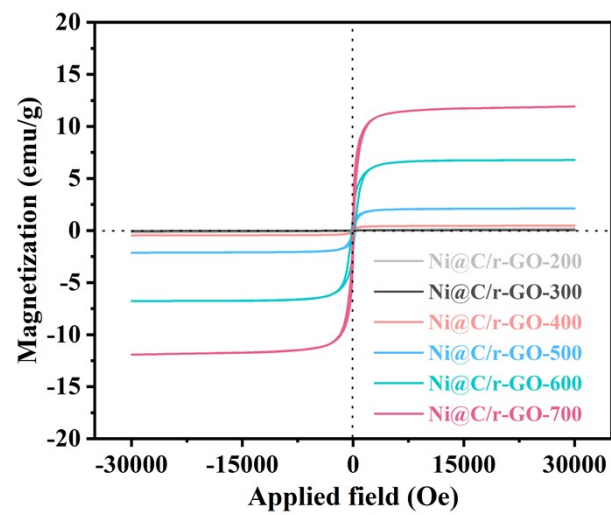**Figure S3** Optical photo of Ni@C/r-GO-700 aerogel on Setaria herb.

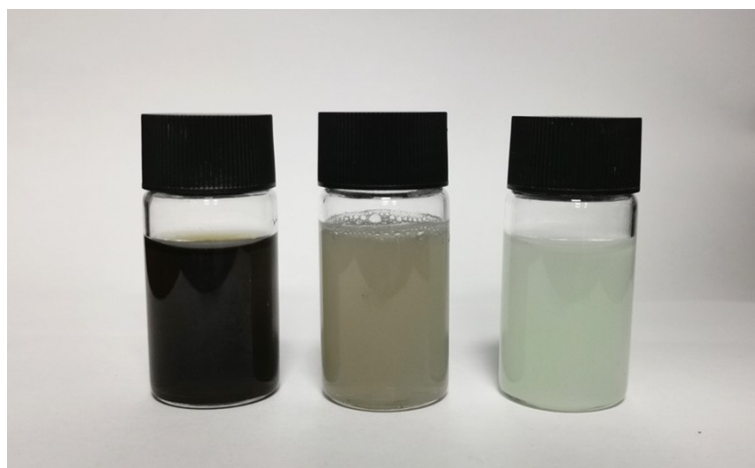**Figure S4**. Magnetization hysteresis loops of the Ni@C/r-GO.

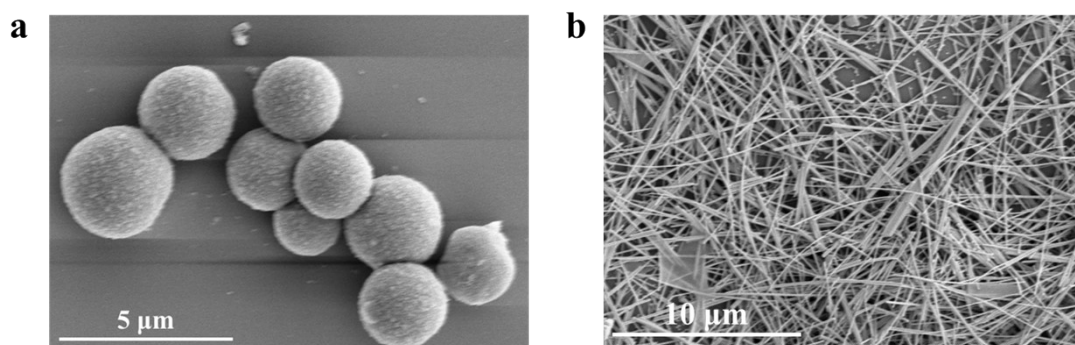**Figure S5** Optical photo of GO, AgNW, and MOF dispersions.
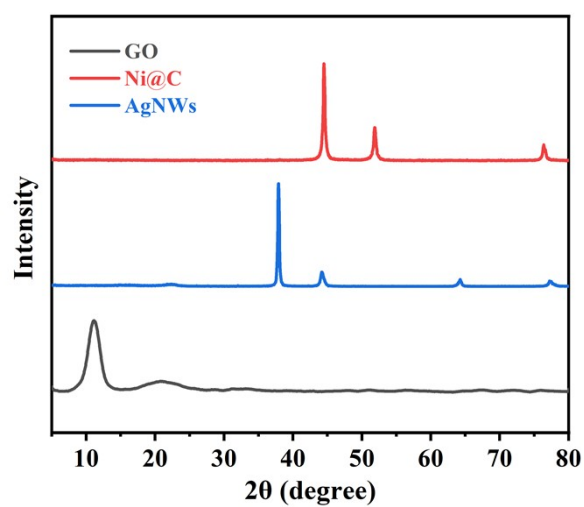

Figure S6 SEM images of (a) Ni@C and (b) AgNW.
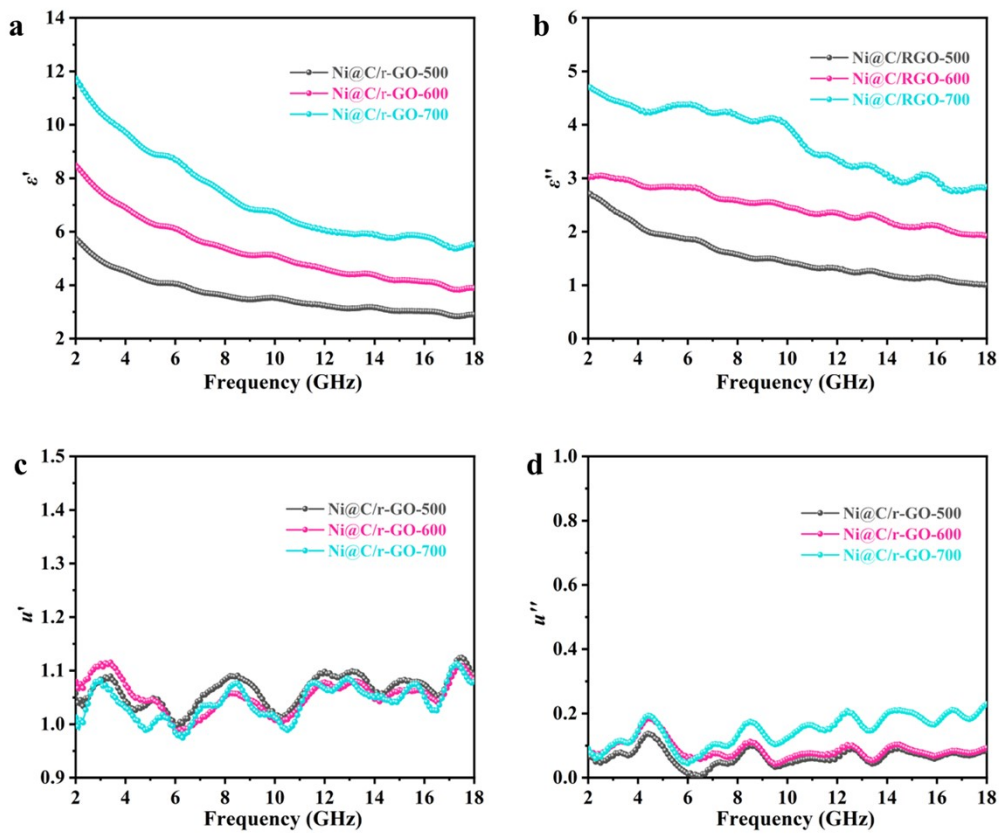

Figure S7 XRD of GO, Ni@C, and AgNW.

Figure S8 The (a) ε', (b) ε'', (c) μ', and (d) μ'' of Ni@C/r-GO-500, Ni@C/r-GO-600 and
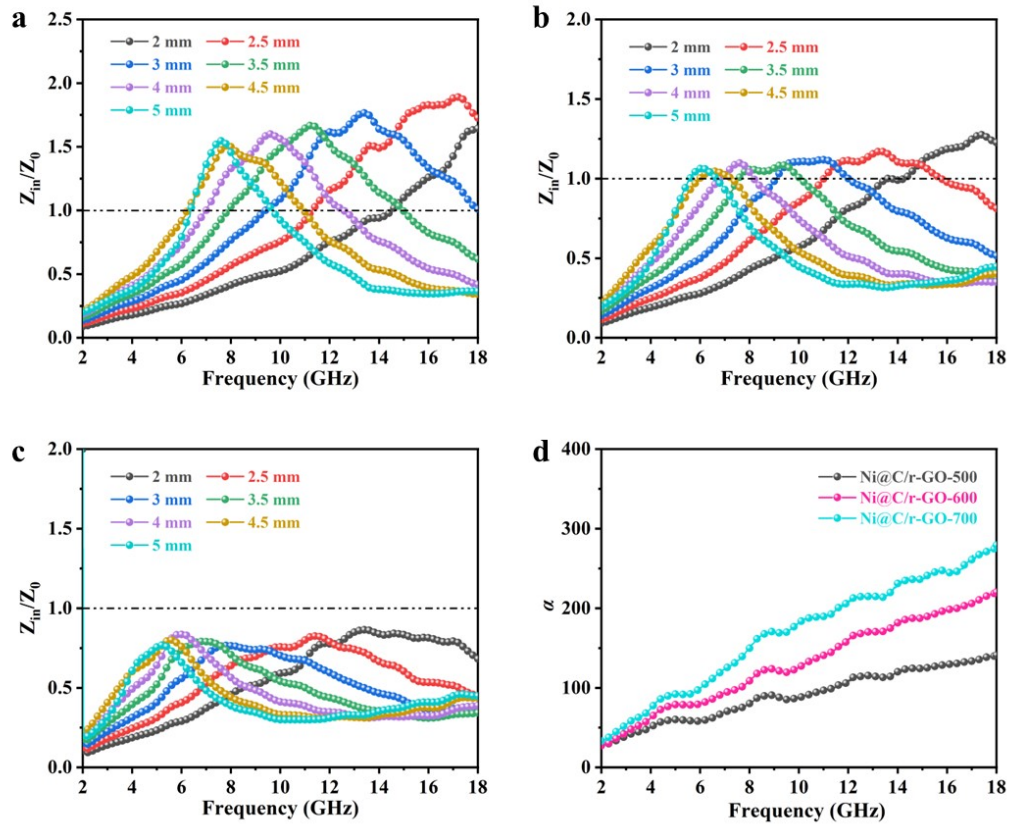
Ni@C/r-GO-700.

Figure S9 Characteristic impedances (Z_{in}/Z_0) of (a) Ni@C/r-GO-500, (b) Ni@C/r-GO-600, and (c) Ni@C/r-GO-700. (d) Attenuation constant (α) of Ni@C/r-GO-500, Ni@C/r-GO-600, and Ni@C/r-GO-700.

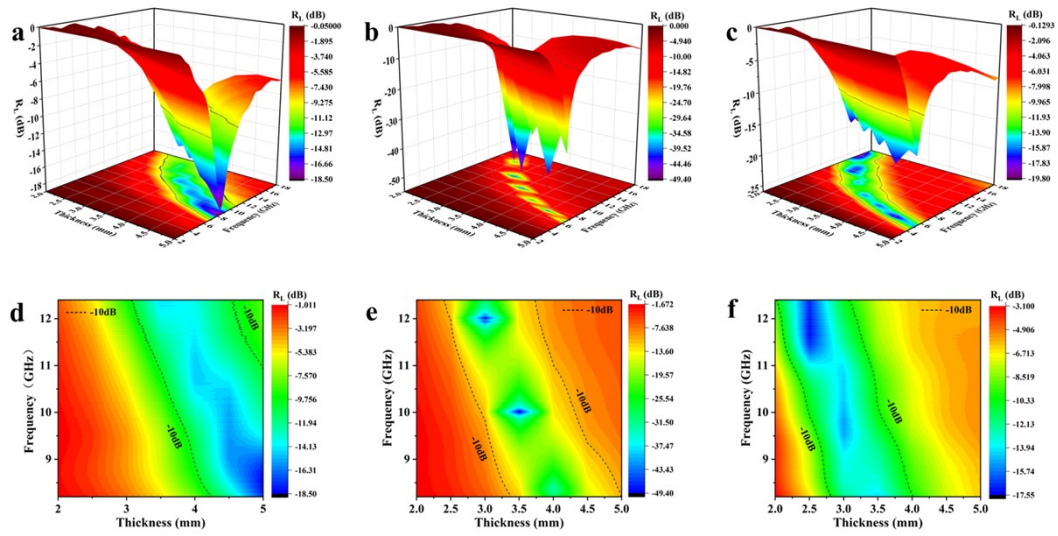**Figure S10** 3D and 2D contour maps of (a, d) Ni@C/r-GO-500, (b, e) Ni@C/r-GO-600, and (c, f) Ni@C/r-GO-700.
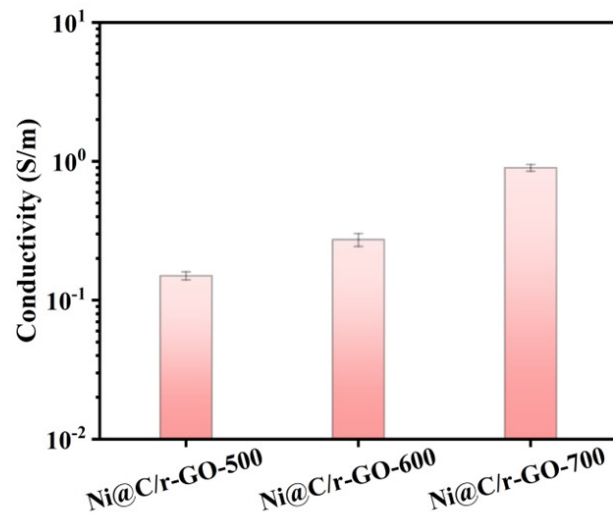
Figure S11 The σ of Ni@C/r-GO-500, Ni@C/r-GO-600, and Ni@C/r-GO-700.
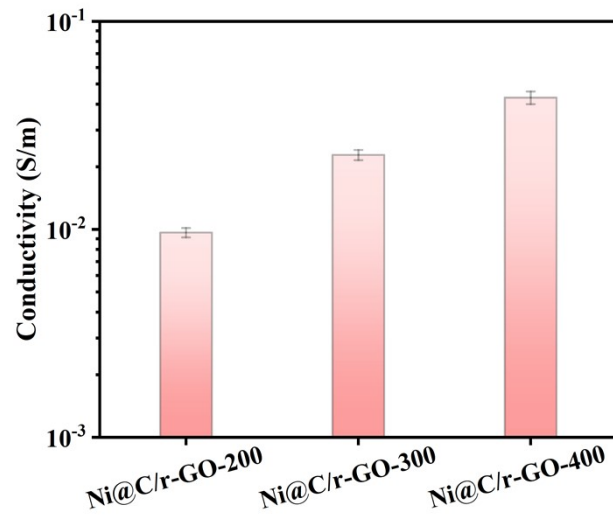
Figure S12 The σ of Ni@C/r-GO-200, Ni@C/r-GO-300, and Ni@C/r-GO-400.
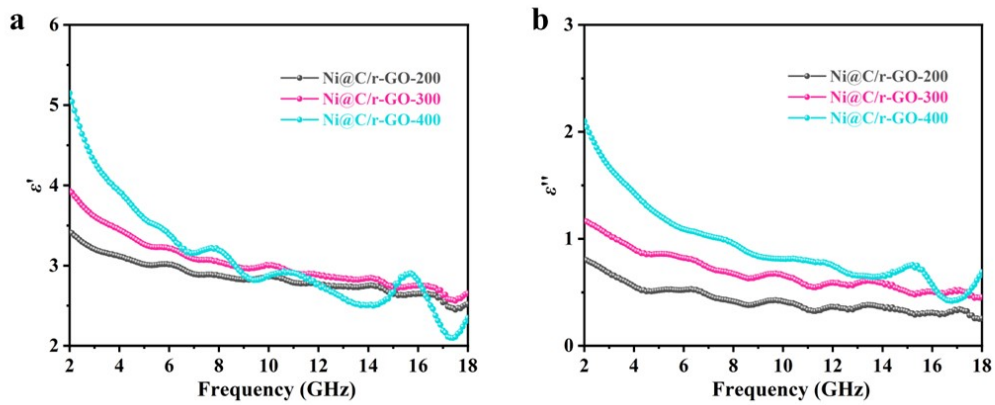
Figure S13 (a) Real part (ε') and (b) Imaginary part (ε'') of Ni@C/r-GO-200, Ni@C/r-GO-300, and Ni@C/r-GO-400.
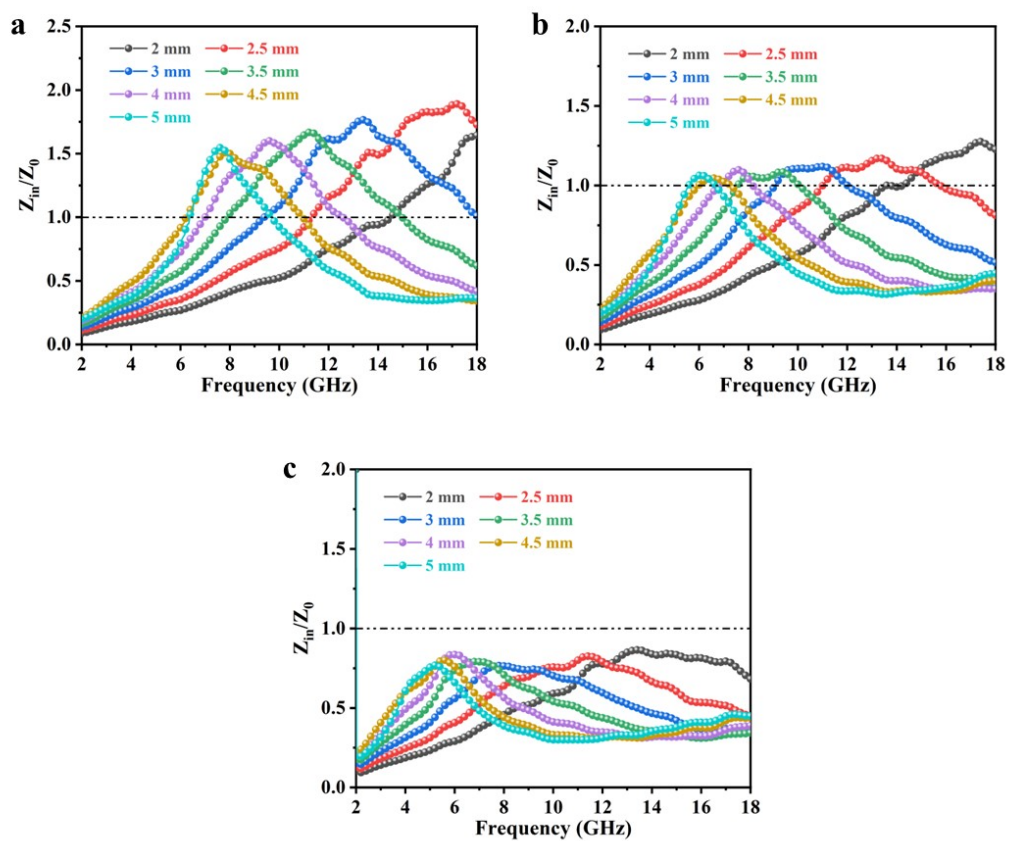
Figure S14 Characteristic impedances (Z_{in}/Z_0) of (a) Ni@C/r-GO-200, (b) Ni@C/r-GO-300, and (c) Ni@C/r-GO-400.
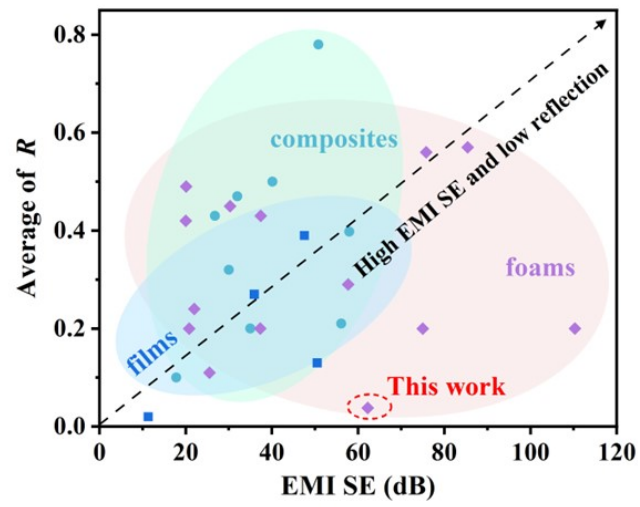
Figure S15 Comparison of average *R* of the shielding materials reported as a function of EMI SE.
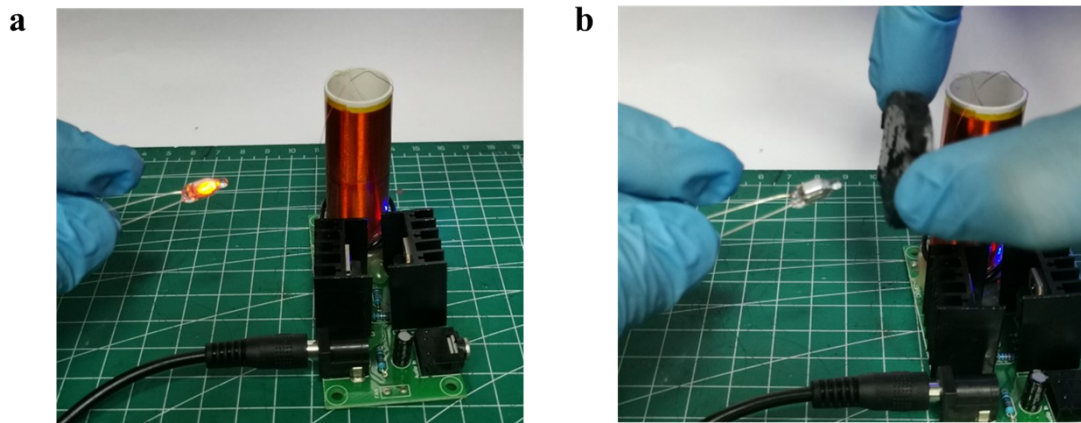
Figure S16 Validation of Tesla coil device on the EMI SE of composite aerogel.
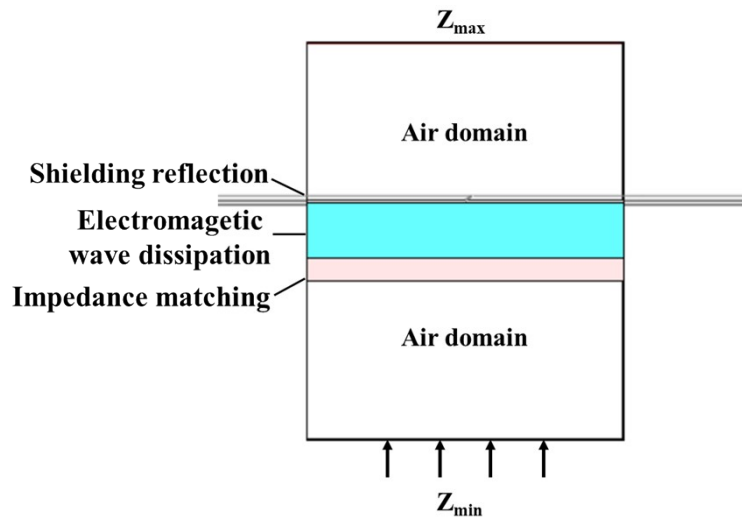
Figure S17 The boundary conditions are unit cell, unit cell and add space in x, y, and z axes respectively, and the solver is a frequency domain solver. The length and width of each model layer is 10 mm and thicknesses of the impedance matching layer, dissipation layer and shielding layer are 1.5 mm, 3.5 mm, and 0.1 mm respectively. Electromagnetic waves propagate from Z_{min} to Z_{max}.
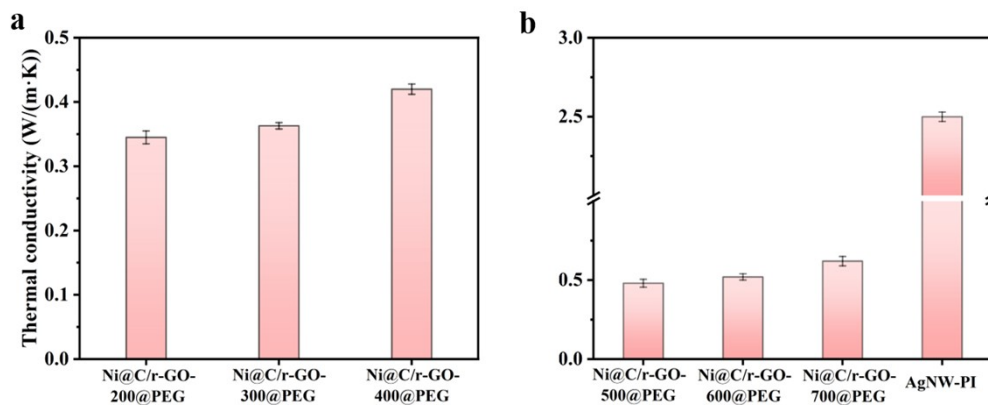
Figure S18 The thermal conductivity of Ni@C/r-GO@PEG and AgNW-PI.

	10S	30S	60S	120S

Nothing

Ni@C/r-GO@PEG
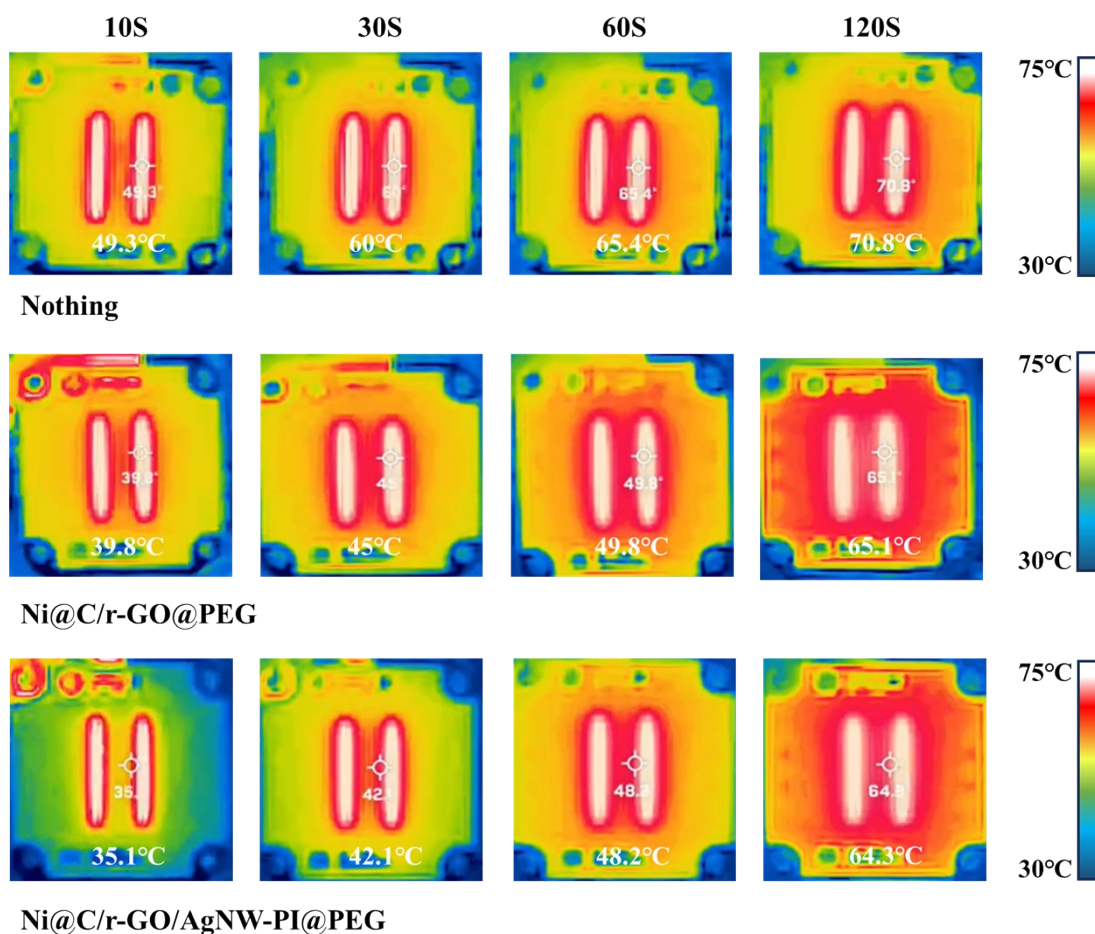
Ni@C/r-GO/AgNW-PI@PEG

Figure S19 IR images showing changes in the LED surface temperature of the Ni@C/r-GO@PEG and Ni@C/r-GO/AgNWs-PI@PEG.
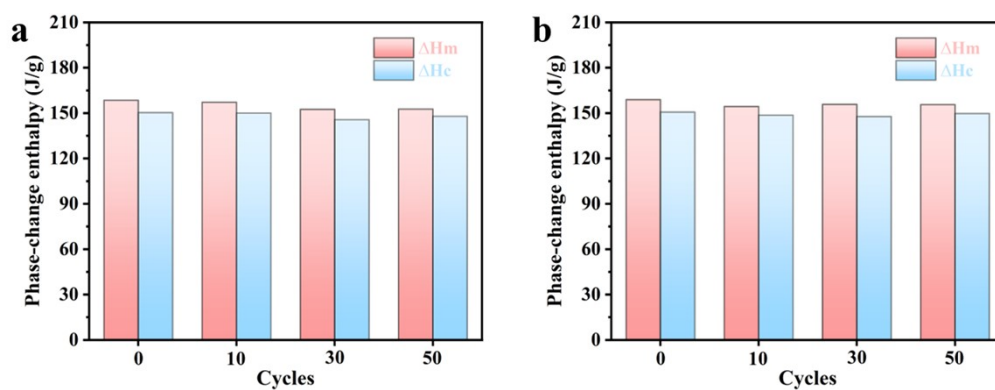
Figure S20 Phase change enthalpy stability of Ni@C/r-GO-300@PEG and Ni@C/r-GO-600@PEG under different heating cycles.
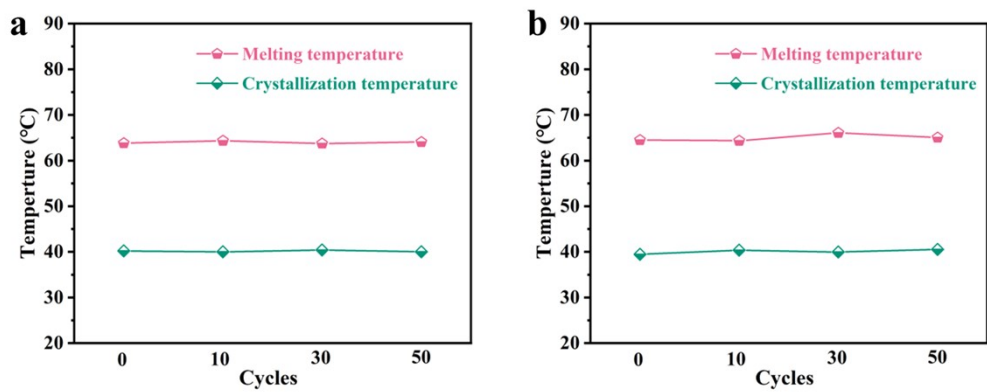
Figure S21 Phase change temperature stability of Ni@C/r-GO-300@PEG and Ni@C/r-GO-600@PEG under different heating cycles.
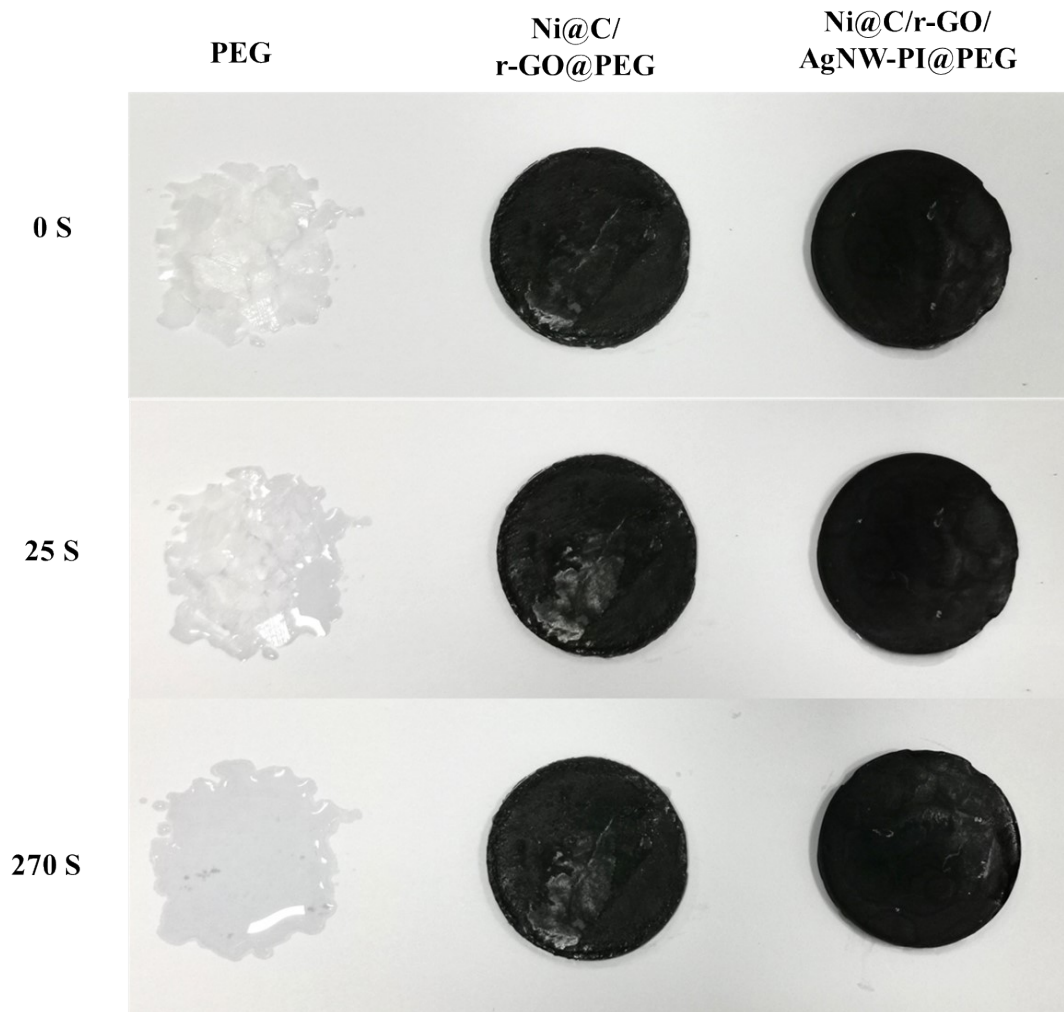
Figure S22 Digital photographs of pure PEG, Ni@C/r-GO@PEG, and Ni@C/r-GO/ AgNW-PI@PEG on the heating stage of 80°C. PEG undergoes partial melting at 25 seconds and complete melting at 270 seconds. In contrast, the composite PCM_S have no leakage during the heating process, and its cylindrical morphology is preserved, proving that excellent encapsulation of PEG in Ni@C/r-GO-X aerogel is achieved.

Table S1 Specific surface area of Ni@C/r-GO.

Sample	S_{BET} (m$^2 \cdot$g^{-1})	V_{pore} (cm$^3 \cdot$g^{-1})	D_{pore} (nm)
Ni@C/r-GO-200	173.96	0.076	1.75
Ni@C/r-GO-300	309.12	0.130	1.68
Ni@C/r-GO-400	213.34	0.123	1.73
Ni@C/r-GO-500	203.12	0.117	2.13
Ni@C/r-GO-600	165.2	0.063	2.21
Ni@C/r-GO-700	105.78	0.056	2.31

Table S2 Phase change behavior of Ni@C/r-GO-300@PEG.

Cycles	ΔH_m (J/g)	T_m (°C)	ΔH_c (J/g)	T_c (°C)	λ (%)	η (%)
0	158.49	63.82	150.38	40.2	90.47	97.28
10	157.19	64.35	150.1	40.01	90.01	96.78
30	152.5	63.74	145.69	40.41	87.34	93.91
50	152.66	64.07	147.92	40.02	88.04	94.67

Table S3 Phase change behavior of Ni@C/r-GO-600@PEG.

Cycles	ΔH_m (J/g)	T_m (°C)	ΔH_c (J/g)	T_c (°C)	λ (%)	η (%)
0	158.94	64.51	150.73	39.48	90.71	96.29
10	154.43	64.34	148.65	40.36	88.76	94.22
30	155.82	66.07	147.75	39.97	88.04	93.46
50	155.65	65.04	149.79	40.54	89.47	94.98

Table S4 Comparison of EMI shielding performance for different materials.

Type	Fillers	Matrix	Thickness (mm)	EMI SE (dB)	SE$_A$ (dB)	SE$_R$ (dB)	R	Ref.
Films	CIP	TPU	0.3	11.3	11.2	0.1	0.02	[1]
	C-ZIF67/GNP	CNF	0.1	50.5	49.9	0.6	0.13	[2]
	GE	PVDF	0.02	47.53	45.36	2.17	0.39	[3]
	Fe$_3$O$_4$@r-GO/MWCNT	WPU		35.9	34.4	1.5	0.27	[4]
Foams	Graphene	PI	0.8	20	17.6	2.4	0.42	[5]
	CNT	PEI	2.2	30.3	27.8	2.5	0.45	[6]
	Graphene	PU	60	57.7	~56.2	<1.5	<0.29	[7]
	Liquid metals	PDMS	0.7	75.8	72.3	3.6	0.56	[8]
	Fe$_3$O$_4$@MWCNTs/Ag	Rubber		85.4	81.7	3.7	0.57	[9]
	Carbon foam/CNT			25.5	25	0.5	0.11	[10]
	CNT/r-GO		0.5	20.1	17.2	2.9	0.49	[11]
	CNTs/Ag	TPU	8.5	68.06	67.8	0.26	0.056	[12]
	MWCNT	Cellulose	2.5	~20.8	~19.7	~1.1	~0.2	[13]
	Ti$_3$C$_2$T		2	75	~74	<1	<0.2	[14]
	GNP	PVDF	3	37.4	34.9	2.5	0.43	[15]
	CNT	N-NR	1.3	37.3	36.3	<1	<0.2	[16]
	CNT	POE	2	21.97	20.76	1.21	0.24	[17]
Composites	CNT/MXene	PVDF	4.15	30	30	2.4×10^{-4}	5.7×10^{-5}	[18]
	Ni@NCNT	CW		57.93	55.33	2.6	0.398	[19]
	G@Fe$_3$O$_4$	PEI	2.5	17.8	17.2	0.5	0.1	[20]
	CCF@CoFe	PI	0.16	32	29.25	2.75	0.47	[21]
	Co/C	CNF	1	56.07	~55.07	<1	~0.21	[22]
	Co/C	CNF		35	~34	<1	~0.2	[23]
	rGO/Fe$_3$O$_4$	Cellulose	0.5	40.1	37.1	~3	~0.5	[24]
	Ni	PC	2	50.8	44.3	6.5	0.78	[25]
	Ni-chains	PVDF	2	26.8	24.3	2.5	0.43	[26]
	SiO$_2$/CNTs/AgNW	PI/CNF	9	110.3	109.0	1.3	0.2	[27]
	Ni@C/r-GO/AgNW	**PEG/PI**	**5**	**62.3**	**62.13**	**0.17**	**0.04**	**This work**

Table S5 Comparison of Enthalpy change efficiency of different materials

Fillers	Composition	Filler content (wt%)	Enthalpy efficiency (%)	References
Ti_3C_2Tx	Ti_3C_2Tx@PDA/PCMs	2	68.75	[28]
BN-OH	PEG/KF/BN-OH	10	86.94	[29]
CNTs+Fe_3O_4	PP/CNTs/Fe_3O_4/PW	10.4	50.59	[30]
GO+GNPs	PEG/HGA	2.25	-	[31]
GNPs+AgNW	PEG@CPG4A6	4.38	93.47	[32]
MXene	P-SAL@MXene	20	76.79	[33]
Ni@C/r-GO/AgNW	**Ni@C/r-GO/AgNw-PI@PEG**	**10**	**97.28**	**This work**

References

1 S. H. Ryu, B. Park, Y. K. Han, S. J. Kwon, T. Kim, R. Lamouri, K. H. Kim and S.B. Lee, *J Mater. Chem. A*, 2022, **10**, 4446-4455.

2 M. Yuan, Y. Fei, H. Zhang, B. Qiu, L. Shen, X. He, M. Liang, S. Zhou, Y. Chen and H. Zou, *Compos. Part B-Eng.*, 2022, **233** 109622.

3 K. Sabira, M. P. Jayakrishnan, P. Saheeda and S. Jayalekshmi, *Eur. Polym. J.*, 2018, **99**, 437-444.

4 A. Sheng, W. Ren, Y. Yang, D. X. Yan, H. Duan, G. Zhao, Y. Liu and Z. M. Li, *Compos, Part A-Appl. S.*, 2020, **129**, 105692.

5 Y. Li, X. Pei, B. Shen, W. Zhai, L. Zhang and W. Zheng, *Rsc Adv.*, 2015, **5**, 24342-24351.

6 D. Feng, P. Liu and Q. Wang, *Ind. Eng. Chem. Res.*, 2020, **59**, 5838–5847.

7 Z. H. Zhou, M. Z. Li, H. D. Huang, L. Li, B. Yang, D. X. Yan and Z. M. Li, *Acs Appl. Mater. Inter.*, 2020, **12**, 18840–18849.

8   M. Zhang, P. Zhang, C. Zhang, Y. Wang, H. Chang and W. Rao, *Appl. Mater. Today.*, 2020, **19**, 100612.

9   J. Yang, X. Liao, G. Wang, J. Chen, W. Tang, T. Wang and G. Li, *J. Mater. Chem. C*, 2019, **8**, 147-157.

10   O. Pitkänen, J. Tolvanen, I. Szenti, Á. Kukovecz, J. Hannu, H. Jantunen and K. Kordas, *Acs Appl. Mater. Inter.*, 2019, **11**, 19331–19338.

11   L. Kong, X. Yin, H. Xu, X. Yuan, T. Wang, Z. Xu, J. Huang, R. Yang and H. Fan, *Carbon*, 2019, **145**, 61-66.

12   Z. Lei, D. Tian, X. Liu, J. Wei, K. Rajavel, T. Zhao, Y. Hu, P. Zhu, R. Sun and C. P. Wong, *Chem. Eng. J.*, 2021, **424**, 130365.

13   H. D. Huang, C. Y. Liu, D. Zhou, X. Jiang, G. J. Zhong, D. X. Yan and Z. M. Li, *J. Mater. Chem. A*, 2015, **3**, 4983-4991.

14   R. Bian, G. He, W. Zhi, S. Xiang, T. Wang and D. Cai, *J. Mater. Chem .C*, 2019, **7**, 474-478.

15   B. Zhao, C. Zhao, M. Hamidinejad, C. Wang, R. Li, S. Wang, K. Yasamin and C. B. Park, *J. Mater. Chem .C,* 2018, **6**, 10292-10300.

16   Y. Zhan, M. Oliviero, J. Wang, A. Sorrentino, G. G. Buonocore, L. Sorrentino, M. Lavorgna, H. Xia and S. Iannace, *Nanoscale*, 2018, **11**, 1011-1020.

17   D. Xu, Q. Wang, D. Feng and P. Liu, *Ind. Eng. Chem. Res.*, 2020, **59**, 1934–1943.

18   L. Wei, J. Ma, L. Ma, C. Zhao, M. Xu, Q. Qi, W. Zhang, L. Zhang, X. He and C. B. Park, *Small Methods*, 2022, **6**, 2101510.

19   M. Cheng, W. Ren, H. Li, X. Liu, S. Bandaru, J. Zhang and X. Zhang, *Compos.*

Part B-Eng., 2021, **224**, 109169.

20 B. Shen, W. Zhai, M. Tao, J. Ling and W. Zheng, *Acs Appl. Mater. Inter.*, 2013, **5**, 11383–11391.

21 J. Li, Y. Ding, Q. Gao, H. Zhang, X. He, Z. Ma, B. Wang and G. Zhang, *Compos. Part B-Eng.*, 2020, **190**, 107935.

22 Y. Fei, M. Liang, T. Zhou, Y. Chen and H. Zou, *Carbon*, 2020, **167**, 575-584.

23 Y. Fei, M. Liang, L. Yan, Y. Chen and H. Zou, *Chem. Eng. J.*, 2020, **392**, 124815.

24 Y. Chen, P. Pötschke, J. Pionteck, B. Voit and H. Qi, *Acs Appl. Mater. Inter.*, 2020, **12**, 22088–22098.

25 Y. Zheng, Y. Song, T. Gao, S. Yan, H. Hu, F. Cao, Y. Duan and X. Zhang, *Acs Appl. Mater. Inter.*, 2020, **12**, 40802–40814.

26 H. Zhang, G. Zhang, Q. Gao, M. Tang, Z. Ma, J. Qin, M. Wang and J. K. Kim, *Chem. Eng. J.*, 2020, **379**, 122304.

27 J. He, M. Han, K. Wen, C. Liu, W. Zhang, Y. Liu, X. Su, C. Zhang and C. Liang, *Compos. Sci. Technol.*, 2023, **231**, 109799.

28 X. Du, J. Qiu, S. Deng, Z. Du, X. Cheng and H. Wang, *ACS Sustainable Chem. Eng.*, 2020, **8**, 5799-5806.

29 Q. Zhang, B. Chen, K. Wu, B. Nan, M. Lu and M. Lu, *Composites, Part A*, 2021, **143**, 106279.

30 X. Li, M. Sheng, S. Gong, H. Wu, X. Chen, X. Lu and J. Qu, *Chem. Eng. J.*, 2022, **430**, 132928.

31 J. Yang, G. Q. Qi, Y. Liu, R. Y. Bao, Z. Y. Liu, W. Yang, B. H. Xie and M. B.

Yang, *Carbon*, 2016, **100**, 693-702.

32   C. Wu, L. Zeng, G. Chang, Y. Zhou, K. Yan, L. Xie, B. Xue and Q. Zheng, *Adv. Compos. Hybrid Mater.*, 2023, **6**, 31.

33   Y. Luo, Y. Xie, H. Jiang, Y. Chen, L. Zhang, X. Sheng, D. Xie, H. Wu and Y. Mei, *Chem. Eng. J.*, 2021, **420**, 130466.